Apert p.Ser252Trp Mutation in FGFR2 Alters Osteogenic Potential and Gene Expression of Cranial Periosteal Cells

Roberto D Fanganiello,[1] Andréa L Sertié,[1] Eduardo M Reis,[2] Erika Yeh,[1] Nélio AJ Oliveira,[1] Daniela F Bueno,[1] Irina Kerkis,[3] Nivaldo Alonso,[4] Sérgio Cavalheiro,[5] Hamilton Matsushita,[5] Renato Freitas,[6] Sergio Verjovski-Almeida,[2] and Maria Rita Passos-Bueno[1]

[1]Departamento de Genética e Biologia Evolutiva, Instituto de Biociências, Universidade de São Paulo, Brazil; [2]Departamento de Bioquímica, Instituto de Química, Universidade de São Paulo, Brazil; [3]Laboratório de Genética, Instituto Butantã, Brazil; [4]Departamento de Cirurgia Plástica, Faculdade de Medicina, Universidade de São Paulo, Brazil; [5]Departamento de Neurologia, Escola Paulista de Medicina, Universidade Federal de São Paulo, Brazil; [6]Centro de Atendimento ao Fissurado, Curitiba, Brazil

Apert syndrome (AS), a severe form of craniosynostosis, is caused by dominant gain-of-function mutations in FGFR2. Because the periosteum contribution to AS cranial pathophysiology is unknown, we tested the osteogenic potential of AS periosteal cells (p.Ser252Trp mutation) and observed that these cells are more committed toward the osteoblast lineage. To delineate the gene expression profile involved in this abnormal behavior, we performed a global gene expression analysis of coronal suture periosteal cells from seven AS patients (p.Ser252Trp), and matched controls. We identified 263 genes with significantly altered expression in AS samples (118 upregulated, 145 downregulated; SNR ≥ |0.4|, $P \leq 0.05$). Several upregulated genes are involved in positive regulation of cell proliferation and nucleotide metabolism, whereas several downregulated genes are involved in inhibition of cell proliferation, gene expression regulation, cell adhesion, and extracellular matrix organization, and in PIK3-MAPK cascades. AS expression profile was confirmed through real-time PCR of a selected set of genes using RNAs from AS and control cells as well as from control cells treated with high FGF2 concentration, and through the analysis of genes involved in FGF-FGFR signaling. Our results allowed us to: (a) suggest that AS periosteal cells present enhanced osteogenic potential, (b) unravel a specific gene expression signature characteristic of AS periosteal cells which may be associated with their osteogenic commitment, (c) identify a set of novel genes involved in the pathophysiology of AS or other craniosynostotic conditions, and (d) suggest for the first time that the periosteum might be involved in the pathophysiology of AS.

Online address: http://www.molmed.org
doi: 10.2119/2007–00027.Fanganiello

INTRODUCTION

Craniosynostosis, the premature fusion of one or more cranial sutures, is a relatively common malformation with an incidence of 1:2.500 births. Apert syndrome (AS [MIM 101200]) is one of the most severe forms of craniosynostosis, accounting for 4.5% of all cases in different populations (1). AS also is characterized by midfacial hypoplasia and severe symmetric bony and cutaneous syndactyly of the hands and feet. Although the coronal suture is closed at birth, the squamosal and the lambdoid suture are opened and the anterolateral fontanelles are much enlarged because of a wide midline calvarial defect. Many other anomalies are associated with AS, such as central nervous system, cardiovascular, urogenital, and dermatologic abnormalities (2–5). Inheritance is autosomal dominant and most cases represent new mutations which are exclusively of paternal origin (6). Early corrective cranial surgical intervention is needed to allow proper brain and skull growth. As a result of continuous bone healing defect, several surgeries are usually necessary during childhood and puberty.

Two activating missense mutations on the fibroblast growth factor 2 receptor (FGFR2) cause the great majority of AS cases: p.Ser252Trp (c.755C > G) and p.Pro253Arg (c.758C > G) (7). They are located in the linker region between immunoglobulin-like loops II and III of the FGFR2: the former is present in about two thirds of the patients and is associated with a more severe craniofacial phenotype and the latter is found in the remaining one third of the patients and is associated with a more severe syndactyly (4). These mutations are present in mesenchymal "FGFR2c" and epithelial "FGFR2b" splice isoforms and they both involve substitutions of bulky side-chain amino acids, which can alter the relative orientation of the ligand-binding sites of this receptor. Either of these changes lead to enhanced FGFR2 ligand binding affinity and decreased specificity (8–10).

FGFR activation by FGFs (fibroblast growth factors) can induce several different cell processes, such as differentiation, proliferation, migration, and apoptosis by

Address correspondence and reprint requests to Maria Rita Passos-Bueno, Rua do Matão 277, Departamento. Genética e Biologia Evolutiva, Instituto de Biociências, USP, São Paulo, SP, 05508-900. Phone: 55-11-30919910; Fax: 55-11-30917419; E-mail: passos(at)ib.usp.br
The first two authors contributed equally to this work.
Submitted April 05, 2007; Accepted for publication June 12, 2007.

activating a variety of intracellular pathways, including MAPK (mitogen-activating protein kinase), PI3K (Phosphoinositide-3 kinase), PKC (protein kinase C), and STAT (signal transducers and activator of transcription) pathways (5). Cellular context and cell nature are important factors that determine the cellular consequences of receptor stimulation. Normal FGFR1-3 signaling also is crucial in the processes of cell growth and differentiation at the cranial sutural margins and alterations in the molecular pathways or in the timing of the activation events can lead to the premature fusion of these margins.

Most of the studies on the cellular consequences of AS mutant FGFR2 activation have been focused on calvarial osteoblasts, both in vitro and in vivo (11–17). Several lines of evidence indicate that the periosteum plays an important role in cranial bone regeneration because removal of this tissue decreases vascularization and calcification of cranial defects in animal models (18,19). However, little or no information about the periosteal cells' role in the pathophysiology of AS is available. We have postulated that the AS cranial periosteal cells may behave abnormally and contribute to enhanced suture ossification, and therefore we decided in the present work to test this hypothesis.

A transcriptional gene expression signature in periosteal AS cells has been previously reported based on the analysis of only one patient harboring the p.Pro253Arg mutation and two controls (20). Therefore, the confirmation of these results with a larger number of patients and controls is clearly warranted. Nonetheless, given that one of the most considerable challenges in the field of molecular medicine is to dissect the mechanisms of isolated cases of genetic diseases, including syndromic craniosynostosis, the identification of gene expression profiles associated with specific Mendelian disorders could become a powerful tool to unravel the underlying causes of this group of diseases.

Thus, the present study aimed to evaluate if p.Ser252Trp FGFR2 mutant periosteal cells present a greater commitment toward osteogenic differentiation, which could contribute to the pathophysiology of AS, and to address if these cells present a transcriptional signature that would be involved in the molecular mechanisms of this syndrome.

SUBJECTS, MATERIAL, AND METHODS

Subjects

During corrective surgery, overlying periosteum from the coronal suture region of seven AS patients (three males and four females aged from three months to 14 years) was meticulously dissected away from surrounding tissues to isolate intact periosteal flaps. Control periosteum was obtained using the same procedure from the coronal suture region of seven subjects (three males and four females aged from 11 months to 13 years) with no evidence of bone disease during craniotomy for removal of brain tumors. The project was approved by the local ethical committee and appropriate informed consent was obtained from each subject or their legal guardians.

The presence of the p.Ser252Trp mutation was confirmed by direct DNA sequencing.

Cell Culture and RNA Isolation

Primary periosteal fibroblast cells derived from the periosteal flaps were grown in fibroblast growth medium (80 percent DMEM, 20 percent fetal bovine serum [FSB] and 2 mmol/L l-glutamine, penicillin, and streptomycin), in a humidified incubator at 37ºC and five percent CO_2. Cells were passaged at near confluence with trypsin-EDTA. All tests were performed between the sixth and the eighth subculture.

Although the primary periosteal fibroblast cells appeared as a homogeneous population of fibroblastoid cells, to further attest that the surgical isolation of periosteum as well as the cell culture expansion procedure were leading to a homogeneous cell sample, immunocytochemistry experiments were performed in two control cell lineages using antibodies specific for mesenchymal cells (SH2 and SH3) and epithelial cells (Cytokeratin 18 and Integrin B1). It was observed that these cells stained homogeneously for the mesenchymal cells markers but not for the epithelial ones. As a positive control, cultured skin fibroblasts from an unaffected subject were used, which stained homogeneously for the epithelial cells markers but not for the mesenchymal cells markers.

Total RNA was isolated from confluent control and AS cells using TRIZOL reagent (Gibco BRL Gaithersburg, MD, USA) and purified with RNeasy mini-columns (Qiagen Valencia, CA, USA). RNA quality and concentration were accessed respectively by 1.5 percent agarose gel electrophoresis and spectrophotometry.

FGFR2 Expression Analysis

To verify the presence of the FGFR2 in AS and control periosteal cells we performed RT-PCR, Western blot, and immunocytochemical experiments.

Expression Analysis of *FGFR2* by RT-PCR

One step RT-PCR (Invitrogen Carlsbad, CA, USA) was performed with 2 μg of total RNA samples from five AS patients and four control subjects and specific primer pairs for each of the two major isoforms of *FGFR2* (*FGFR2*b and *FGFR2*c). The same forward primer (FGFR2-6F: 5′-agtgtggtcccatctgacaag-3′) was combined with a reverse primer specific for either the *FGFR2b* (FGFR2b-9R: 5′-ggcctgccctatataattgga-3′) or *FGFR2c* (FGFR2c-10R: 5′-atagaattacccgccaagcac-3′) isoform. A total of 35 cycles of amplification were performed. Reaction products were resolved alongside a 100-bp ladder on 1.5 percent agarose gel.

Western Blot and Immunocytochemical Experiments

Cell lysates from three AS patients and from three control subjects were prepared in RIPA Buffer (5 mM Tris-HCl pH7.4, 150 mM NaCl, 1 mM EDTA, 0.1 percent SDS, 0.5 percent sodium deoxycholate, one percent Nonidet 40) and 500 μg of protein were subject to Western blot analysis using a dilution of 1:250 of primary antibody BEH (H-80: sc-20734,

Santa Cruz Biotechnology Santa Cruz, CA, USA), and 1:1000 of anti-rabbit alkaline-phosphatase conjugated secondary antibody. For the immunocytochemical experiments, cells were treated with paraformaldehyde (four percent during 30 min) and labeled with 1:100 of the first antibody BEH and 1:100 of the second anti-rabbit-Cy3 antibody. As positive control we used the murine adenocortical Y1 cells (kindly provided by Dr. Hugo Armelin). Control staining without primary antibody was used as negative control.

In Vitro Osteogenic Differentiation

To induce osteogenic differentiation, periosteal fibroblasts from two AS patients and two controls were cultured for three weeks in DMEM ten percent FBS, 0.1 mM dexamethasone, 50 mM ascorbate-2-phosphate, 10 mM β-glycerophosphate, 0.1 percent antibiotic, with media changes every three to four days. After 21 days, calcified matrix production was analyzed by von Kossa staining as previously described (21).

Microarray Assays, Normalization, and Statistical Analyses

Gene expression experiments were performed using CodeLink bioarray systems (GE Healthcare Buckinghamshire, UK) according to manufacturer's protocols. In brief, first-strand cDNA was produced using 2 μg of total RNA from each sample, Superscript II reverse transcriptase and a T7-poly-dT primer. Second-strand cDNA was produced using RNase H and *E. coli* DNA polymerase I. Double-stranded cDNA was purified on a QIAquick column (Qiagen) and biotin-labeled cRNA targets were generated by an in vitro transcription reaction using T7 RNA polymerase and biotin-11-UTP (Perkin Elmer-Foster City, CA, USA). Fragmented cRNA from each sample was hybridized to CodeLink microarrays containing approximately 20,000 (20K, five samples) or 55,000 (55K, nine samples) 30-mer probes overnight at 37°C in a shaking incubator at 300 rpm. After post-hybridization washes, hybridized targets were revealed by incubating the arrays with a Cy5-Streptavidin conjugate. The reagents used in the synthesis and fragmentation of cRNA were provided in the CodeLink expression assay kit (GE Healthcare). Signal of the Cy5-dye from hybridized targets were detected with a GenePix 4000B scanner (Axon Instruments Foster City, CA, USA). CodeLink Expression Analysis software (GE Healthcare) was used to obtain background-subtracted spot intensities from microarray images. A set of 19,683 cDNA probes present in both the 20K and 55K arrays were analyzed. From these, only 9,543 probes that had valid measurements (i.e. were detected above the average array background as determined by a set of negative controls represented in the CodeLink arrays) in at least six out of seven samples from AS or control samples were further analyzed. To make experiments comparable, intensity data from different hybridizations were normalized by two different methods: (i) trimmed mean excluding the 20 percent of spots with higher and lower intensities, or (ii) Lowess, local weighted scatter-plot smoothing (22). Data adjusted by Lowess to a reference file resulted in lower coefficient of variation values across all samples and were used in further analyses. To identify gene expression signatures of AS, a Signal-to-Noise Ratio (SNR) metric (23) was used to compare the expression intensity data from AS samples to control samples. The SNR parameter essentially is a measure of signal strength relative to background noise. The distance between the two groups was measured by a signal-(expression intensity) to-noise (variation) ratio. The signal-to-noise comparison gives an indication of the level of separation for the means of the two distributions defining the gene intensities of the two groups, and it was calculated as SNR = $\sqrt{(\mu_1 - \mu_2)^2} / (SD_1 + SD_2)$, where μ_1 and μ_2 are the mean intensities of Apert and control groups, respectively, and SD_1 and SD_2 the corresponding standard deviations. For each gene, higher absolute SNR values indicate a higher difference of expression between AS and control samples with a lower dispersion within each group. A cutoff SNR ≥ |0.4| was used to select differentially expressed genes. Statistical significance of the differential expression (*P* values) was ascertained by bootstrap resampling, i.e. by re-calculating SNR values following 10,000 random permutations of sample labels and computing the frequency at which each SNR value measured in the original set was observed in the randomly permuted data (24). The robustness of identified AS gene expression signature was evaluated by sample leave-one-out cross-validation (25). Essentially, one sample is removed and a new set of significantly altered genes is determined using the remainder samples. This procedure was repeated for each one of the 14 AS/control samples and the frequency at which each gene appears in the various "leave-one-out" datasets at a given significance ($P \leq 0.05$) was annotated.

The reproducibility of the gene expression measurements was assessed by generating two independent replicate target preparations for each of two AS patients and one control and hybridization of the replicates to separate 55K or 20K microarrays, the two types of microarray platforms used in our gene expression experiments. Pair-wise comparison using the Pearson correlation was applied to compare the intensity values from the 19,683 probes common to both CodeLink platforms. Intensity values from the probes common to both microarray platforms were highly correlated between sample replicates (average Pearson correlation = 0.95 ± 0.01) among the three sets of hybridizations. This result confirms that intensity measurements obtained in the different platforms can be compared without any significant loss in accuracy. In addition, the average correlation measured in pairwise analyses with data from all 14 different samples was 0.83 ± 0.07.

Reverse Transcription Reactions and Quantitative Real-time PCR

Complementary DNA (cDNA) was produced from four μg of total RNA using Superscript II reverse transcription kit (Invitrogen). Quantitative real-time PCR (qRT-PCR) was performed using approximately 200 ng

Table 1. Sequence of the primers used in the quantitative Real Time PCR experiments.

Gene	Forward sequence	Reverse sequence
CENPN	TCAGTGATGCTGCCCTGTTAGA	AGTGATGCTGCCCTGTTAGACA
STMN1	GGCAGGACTTTCCTTATCCCA	GGCAGGACTTTCCTTATCCCA
SPAG5	GAGTTCAAGGAGGTGCTGAAGA	TGTCTGGAGGTCCTGCTATTTC
RMM2	CTTTGTCATCTTCCCCATCGAG	TGCTGAATGTCCTTGGAGAGGT
HIP2	GAGTTCAAGGAGGTGCTGAAGA	TGTCTGGAGGTCCTGCTATTTC
EEF1B2	TTCGGAGACCTGAAAAGCCCT	CGGCTTCAAATACTGCCACATC
HPRT1	TGACACTGGCAAAACAATGCA	GGTCCTTTTCACCAGCAAGCT
SDHA	TGGGAACAAGAGGGCATCTG	CCACCACTGCATCAAATTCATG

of cDNA and SYBR Green PCR master mix in an ABI Prism 7100 system (Applied Biosystems Foster City, CA, USA). The PCR conditions were: 94°C for 15 s, 58°C for 30 s, and 72°C for 30 s for 40 cycles.

Samples from four AS and four controls were run in triplicates, and the threshold suggested by the instrument software was used to calculate Ct. To normalize the readings we used Ct values from *HPRT1* (*Hypoxanthine phosphoribosyltransferase 1)* and *SDHA* (*succinate dehydrogenase complex, subunit A)* as internal controls in each run, obtaining a delta Ct value for each tested gene (*STMN1*, *SPAG5*, *RRM2*, *HIP2*, *CENPN*, *EEF1B2*). Primers used in this study are summarized in Table 1 as supplementary information.

Exogenous FGF2 Treatment

Control periosteal fibroblasts were grown to about 80 percent confluence in six 25 cm^2 cell culture bottles as described. Cells were washed with PBS and then were serum starved for 24 h in DMEM not supplemented with FBS. After this period, control cells (three bottles) were treated with DMEM containing 0.5 percent FBS and experimental cells (three bottles) were treated with DMEM 0.5 percent FBS and recombinant bovine FGF2 (provided by Dr. Hugo Armelin) to a final concentration of 36 ng/mL (or 2000 pM – at this high concentration phosphorylation of both wild type and mutant FGFR2c was similar, as observed by 9). Control and experimental cells were harvested at three, six, and 24 h after addition of FGF2, and had its total RNA isolated and purified as described. cDNA was obtained by reverse transcription of two μg of total RNA using Superscript II (Invitrogen). qRT-PCR was used to measure expression levels of *STMN1*, *SPAG5*, *RRM2*, *HIP2*, *CENPN*, *EEF1B2* after FGF2 stimulation.

RESULTS

Morphology and FGFR2 Expression Analysis in Periosteal Cells

Cultured coronal suture periosteal cells from wild type controls and AS patients appeared microscopically to be a homogeneous population of adherent fibroblast-like cells, which exhibited neither morphology alteration nor significant cell death after several passages.

As expected for a homogeneous cellular population of periosteal cells with mesenchymal origin, we observed only the expression of the *FGFR2c* isoform in control and AS periosteal cells, with no apparent difference between these two, as determined by RT-PCR. FGFR2 protein also was detected in similar amounts both in control and AS cells (data not shown).

Differentiation of Periosteal Fibroblasts to the Osteoblast Cell Lineage

To address if AS periosteal cells present a greater osteogenic potential, control and AS cells (Figure 1A) were treated with osteogenic induction medium. We found that the potentiality to differentiate to osteogenic lineage varied significantly between control and AS cellular

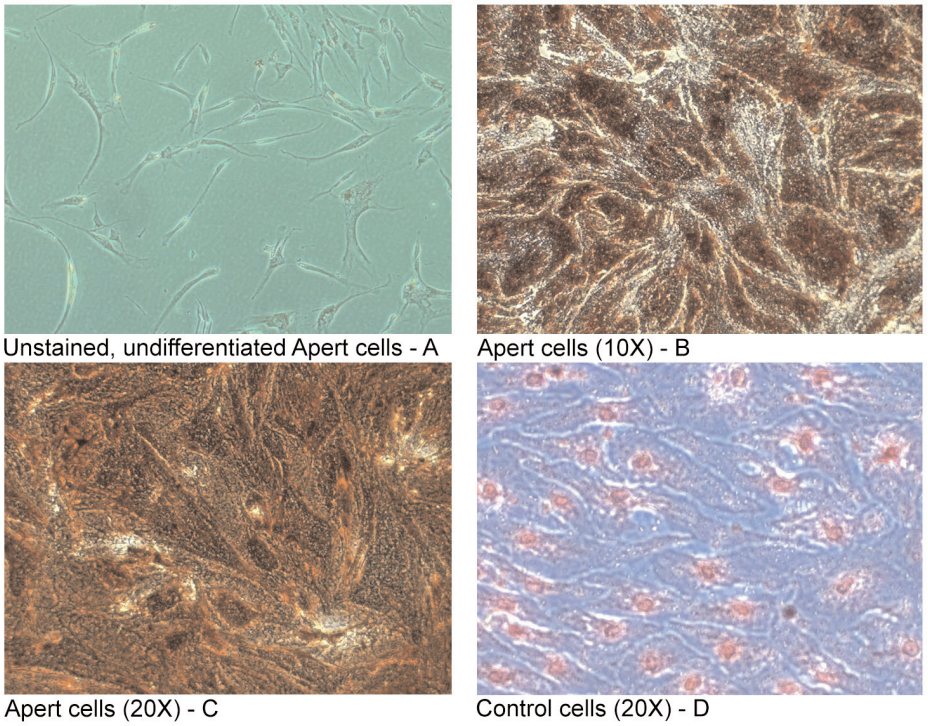

Figure 1. (A) Morphology of undifferentiated AS periosteal cells. (B and C) Osteogenic differentiation of periosteal cells after 21 days of culture in osteogenic medium. Secretion of a calcified extracellular matrix was clearly observed. (D) Control cells after 21 days of osteogenic induction without signals of osteogenic differentiation (mineralized matrix are absent). Differentiation was accessed by von Kossa staining.

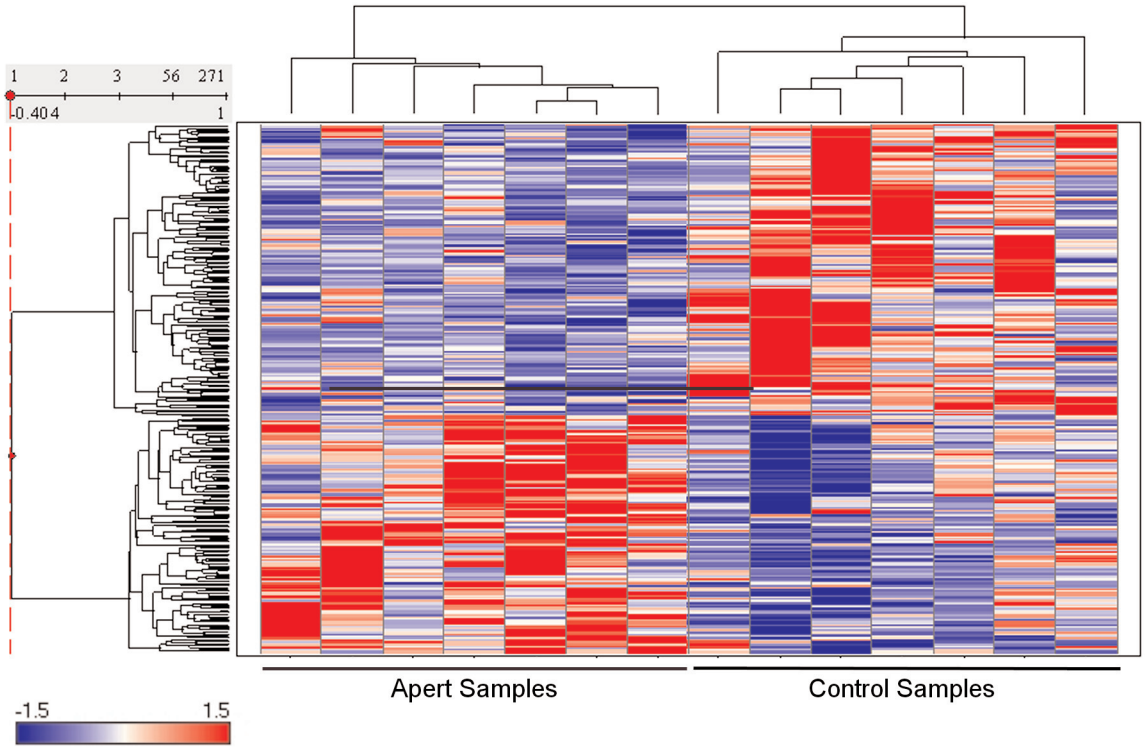

Figure 2. Hierarchical clustering of a 263 gene expression signature of AS samples relative to normal control samples. Individual genes are represented in lines and different samples are represented in rows. Expression level of each gene is represented by the number of standard deviations above (red) or below (blue) the average value for that gene across all samples. Color intensity is proportional to the number of standard deviations in the range –1.5 to 1.5, as indicated by the color-coded bar at the bottom of the figure.

populations. Four days after the beginning of treatment, an osteoblast-like phenotype was observed in AS cells, while control cells maintained the fibroblast-like morphology. After 21 days of treatment, we observed several areas positive for calcium staining by the von Kossa reaction in AS cells (Figure 1 B and C), but not in control cells (Figure 1 D).

Differential Gene Expression

To verify whether there is an expression signature associated with the presence of the p.Ser252Trp mutation, which could explain the altered mutant cell behavior, we performed genome-wide expression analysis with RNA samples from seven AS patients and seven gender- and age-matched controls using either 55K or 20K microarray platforms. We found 9,543 transcripts (out of 19,683 transcripts under analysis) that were expressed in at least six out of seven samples from AS or control subjects. The average expression levels of 263 genes were found to be significantly altered in AS samples when compared with normal subjects (118 genes upregulated and 145 downregulated) (Figure 2, Table 2 – supplementary information), using as thresholds an absolute SNR ≥ |0.4| and $P \leq 0.05$ (see Methods section for details).

Submitting the 263 differentially expressed genes to the KEGG Pathway Database, the Gene Ontology Database (AmiGO), and the NCBI (Gene) database, we found that 186 of them have a known or inferred function. Among them, we found 98 genes that could be grouped in the following functional categories: regulation of cell proliferation (36 genes; among them, 28 and eight genes are involved in positive and negative regulation of cell proliferation, respectively), nucleotide metabolism (ten genes), regulation of gene expression (32 genes), apoptosis (17 genes), cell adhesion (13), extracellular matrix component or biogenesis (seven genes), and MAPK pathways (16 genes) (Table 3). Some genes belong to more than one functional category. These categories were selected because they contain the largest numbers of genes, and because genes with related biological functions already were associated to FGFR2 signaling.

From this analysis, we observed that the most abundant classes of transcripts were those associated with regulation of cell proliferation and regulation of gene expression. In addition, among the 98 genes functionally classified, 45 were upregulated while 53 were downregulated in AS cells. Among the upregulated genes, the majority belong to positive regulation of cell proliferation and nucleotide metabolism categories (29/45 genes or ~64.4%) (Table 3).

Table 2. 263 transcripts differentially expressed in AS cells as compared with control samples. Transcripts are ordered by their Apert-to-control ratios (Log 2).

Gene (Official Symbol)	Gene name	Accession number	SNR[a]	*P* value	Apert-to-control Ratio (Log2)	x-fold down-regulated in Apert
DKFZp434B1231[b]	eEF1A2 binding protein	NM_178275.3	–0.86	0.010	–2.66	6.31
TNNT1[c]	troponin T type 1 (skeletal, slow)	F36108.1	–0.662	0.017	–2.45	5.46
TNXB[b]	tenascin XB	NM_032470.2	–0.769	0.015	–2.32	4.98
CYHR1[b]	cysteine/histidine-rich 1	AB007965.1	–1.013	0.010	–2.21	4.62
RTN4RL1[b]	reticulon 4 receptor-like 1	AL834409.1	–0.812	0.023	–1.83	3.57
CCRL1	chemokine (C-C motif) receptor-like 1	NM_016557.2	–0.65	0.035	–1.77	3.42
NISC_np07a06y1 NICHD_HS_Ut1	NISC_np07a06y1 NICHD_	CB215524.1 HS_Ut1 cDNA clone IMAGE:5936938 5′	–0.422	0.047	–1.76	3.39
PCNXL2[b]	pecanex-like 2 (Drosophila)	NM_014801.2	–0.773	0.023	–1.75	3.36
CFB	complement factor B	NM_001710.3	–0.678	0.027	–1.74	3.34
DDIT4[b]	DNA-damage-inducible transcript 4	NM_019058.1	–0.564	0.022	–1.71	3.28
RARRES3[b]	retinoic acid receptor responder (tazarotene induced) 3	NM_004585.2	–0.773	0.022	–1.64	3.12
ZC3H12A	zinc finger CCCH-type containing 12A	NM_025079.1	–0.499	0.047	–1.62	3.08
PIK3C2B[c]	phosphoinositide-3-kinase, class 2, β polypeptide	NM_002646.2	–0.903	0.004	–1.54	2.91
TP53I11	tumor protein p53 inducible protein 11	BC045666.1	–0.702	0.026	–1.48	2.79
GBP2	guanylate binding protein 2, interferon-inducible	NM_004120.3	–0.689	0.031	–1.43	2.69
ChGn[c]	chondroitin beta1,4 N-acetylgalactos-aminyltransferase	NM_018371.3	–0.819	0.015	–1.42	2.68
ZNF385[b]	zinc finger protein 385	NM_015481.1	–0.955	0.011	–1.38	2.61
UI-E-CQ1-aew-i-06-0-UIr1 UI-E-CQ1	UI-E-CQ1-aew-i-06-0-UIr1 UI-E-CQ1 cDNA clone UI-E-CQ1-aew-i-06-0-UI 5′	BM695626.1	–0.661	0.042	–1.37	2.59
PDGFRA	platelet-derived growth factor receptor, α polypeptide	NM_006206.2	–0.653	0.045	–1.34	2.53
LRRC17[b]	leucine rich repeat containing 17	NM_005824.1	–0.643	0.039	–1.25	2.38
yr27d04r1	yr27d04r1 Soares fetal liver spleen 1NFLS cDNA clone IMAGE:206503 5′	H59349.1	–0.708	0.039	–1.25	2.38
MGC:71335[b]	cDNA clone MGC:71335 IMAGE:6088873	BC067086.1	–0.825	0.009	–1.25	2.37
FLJ43880[c]	cDNA FLJ43880 fis, clone TESTI4009022	AK125868.1	–0.796	0.017	–1.24	2.36
ADAM33	ADAM metallopeptidase domain 33	NM_153202.1	–0.709	0.027	–1.22	2.33
RC6-HT0840-150800-022-D11 HT0840	RC6-HT0840-150800-022-D11 HT0840 Homo sapiens cDNA	BE719128.1	–0.678	0.031	–1.22	2.33
FXYD1	FXYD domain containing ion transport regulator 1 (phospholemman)	NM_021902.2	–0.578	0.044	–1.20	2.29
MAF	v-maf musculoaponeurotic fibrosarcoma oncogene homolog (avian)	NM_005360.2	–0.568	0.044	–1.19	2.29

Continued

TABLE 2—*Continued*

ABI3BP[c]	ABI gene family, member 3 (NESH) binding protein	NM_015429.2	–0.705	0.012	–1.17	2.26
UI-E-DW1-ahc-b-11-0-UIr1 UI-E-DW1[c]	UI-E-DW1-ahc-b-11-0-UIr1 UI-E-DW1 cDNA clone UI-E-DW1-ahc-b-11-0-UI 5′	BM712072.1	–0.854	0.008	–1.14	2.21
MTSS1[b]	metastasis suppressor 1	NM_014751.2	–0.731	0.009	–1.14	2.20
CLDN15[b]	claudin 15	NM_014343.1	–0.714	0.022	–1.13	2.19
GANAB	glucosidase, alpha; neutral AB	NM_198334.1	–0.719	0.020	–1.13	2.19
C1QTNF1[c]	C1q and tumor necrosis factor related protein 1	NM_030968.2	–0.672	0.017	–1.13	2.18
ATF3	activating transcription factor 3	NM_004024.2	–0.619	0.049	–1.10	2.14
C17orf58[c]	chromosome 17 open reading frame 58	NM_181655.1	–0.813	0.007	–1.10	2.14
P2RY6[c]	pyrimidinergic receptor P2Y, G-protein coupled, 6	NM_004154.3	–0.814	0.021	–1.08	2.12
ADAM8[c]	a disintegrin and metalloproteinase domain 8	NM_001109.1	–0.628	0.044	–1.06	2.08
PNRC1	proline-rich nuclear receptor coactivator 1	NM_006813.1	–0.902	0.008	–1.05	2.07
FLJ23438[b]	cDNA: FLJ23438 fis, clone HRC13275	AK027091.1	–0.738	0.016	–1.04	2.06
BTN3A3[c]	butyrophilin, subfamily 3, member A3	NM_197974.1	–0.833	0.009	–1.03	2.05
UI-H-EU0-azp-a-24-0-UIs1 NCI_CGAP_Car1[b]	UI-H-EU0-azp-a-24-0-UIs1 NCI_CGAP_Car1 cDNA clone IMAGE: 5851679 3′	BQ181011.1	–0.716	0.009	–1.01	2.01
CREB5[b]	cAMP responsive element binding protein 5	NM_004904.1	–0.9	0.010	–1.00	2.00
HLA-G	HLA-G histocompatibility antigen, class I, G	NM_002127.3	–0.721	0.028	–0.99	1.99
MATN2	matrilin 2	NM_030583.1	–0.743	0.027	–0.96	1.95
HHLA2	HERV-H LTR-associating 2	NM_007072.2	–0.488	0.024	–0.95	1.93
HLA-F	major histocompatibility complex, class I, F	NM_018950.1	–0.619	0.039	–0.95	1.93
TXNIP	thioredoxin interacting protein	NM_006472.1	–0.604	0.034	–0.94	1.92
KLF11	Kruppel-like factor 11	NM_003597.4	–0.493	0.039	–0.92	1.89
ARID5A	AT rich interactive domain 5A (MRF1-like)	NM_006673.2	–0.526	0.042	–0.92	1.89
PERP	PERP, TP53 apoptosis effector	NM_022121.2	–0.602	0.042	–0.92	1.89
HHLA1	HERV-H LTR-associating 1	NM_005712.1	–0.661	0.031	–0.92	1.89
GYPC[b]	glycophorin C (Gerbich blood group)	NM_002101.3	–0.578	0.046	–0.91	1.88
NUCB1	nucleobindin 1	NM_006184.3	–0.618	0.026	–0.89	1.86
LGALS3BP[b]	lectin, galactoside-binding, soluble, 3 binding protein	NM_005567.2	–0.784	0.014	–0.89	1.85
FLJ20099[b]	cDNA FLJ20099 fis, clone COL04544	AK000106.1	–0.711	0.023	–0.89	1.85
TMEM142C[b]	transmembrane protein 142C	NM_152288.1	–0.803	0.011	–0.87	1.83
ATXN2L	ataxin 2-like	NM_007245.2	–0.596	0.046	–0.87	1.83
PAQR6[b]	progestin and adipoQ receptor family member VI	NM_024897.2	–0.63	0.040	–0.87	1.83
SPTBN1	spectrin, beta, non-erythrocytic 1 (SPTBN1)	NM_003128.1	–0.62	0.049	–0.87	1.83
MGC15875[b]	hypothetical protein MGC15875 (MGC15875)	NM_032921.1	–0.894	0.013	–0.86	1.81
MAPK8IP1	mitogen-activated protein kinase 8 interacting protein 1	NM_005456.2	–0.642	0.037	–0.86	1.81

Continued

TABLE 2—*Continued*

ANKZF1	ankyrin repeat and zinc finger domain containing 1	NM_018089.1	–0.673	0.036	–0.85	1.81
CCBE1	collagen and calcium binding EGF domains 1	NM_133459.1	–0.602	0.034	–0.85	1.81
DKFZp779O 1626	mRNA; cDNA DKFZp779O1626 (from clone DKFZp779O1626)	BX648538.1	–0.676	0.027	–0.83	1.78
CA12	carbonic anhydrase XII	AK000158.1	–0.612	0.040	–0.83	1.78
NFIL3[b]	nuclear factor, interleukin 3 regulated	NM_005384.1	–0.803	0.012	–0.83	1.77
IFITM3	interferon induced transmembrane protein 3 (1-8U)	NM_021034.1	–0.604	0.033	–0.83	1.77
SLC27A1	solute carrier family 27 (fatty acid transporter), member 1	NM_198580.1	–0.621	0.047	–0.81	1.75
LAMP1	lysosomal-associated membrane protein 1	NM_005561.2	–0.648	0.037	–0.80	1.74
BCL3	B-cell CLL/lymphoma 3	NM_005178.2	–0.671	0.039	–0.79	1.73
R15896 ya 47b07.r1	R15896 ya47b07.r1 Soares infant brain 1NIB cDNA clone IMAGE:53125 5′ similar to SP:S37009 S37009 TRANSPOSASE - ALMOND ;	R15896.1	–0.645	0.037	–0.79	1.73
ZFP64[b]	zinc finger protein 64 homolog (mouse)	NM_018197.2	–0.795	0.017	–0.78	1.72
SWAP-70[b]	SWAP-70 protein	AB014540.1	–0.708	0.028	–0.77	1.71
P2RX4	purinergic receptor P2X, ligand-gated ion channel, 4	NM_002560.2	–0.69	0.032	–0.77	1.71
BMP1	bone morphogenetic protein 1 (BMP1)	NM_006129.2	–0.598	0.048	–0.76	1.69
SLC25A37	solute carrier family 25, member 37	NM_016612.1	–0.607	0.039	–0.75	1.68
NUB1[b]	negative regulator of ubiquitin-like proteins 1	NM_016118.3	–0.68	0.011	–0.75	1.68
ACADS	acyl-Coenzyme A dehydrogenase, C-2 to C-3 short chain	NM_000017.1	–0.669	0.046	–0.74	1.67
RELB	v-rel reticuloendotheliosis viral oncogene homolog B, nuclear factor of kappa light polypeptide gene enhancer in B-cells 3 (avian)	NM_006509.2	–0.682	0.033	–0.74	1.67
PPARA[b]	peroxisome proliferative activated receptor, α	NM_032644.1	–0.753	0.009	–0.74	1.67
ELL3[b]	elongation factor RNA polymerase II-like 3	NM_025165.1	–0.791	0.006	–0.74	1.67
BCL6[c]	B-cell CLL/lymphoma 6 (zinc finger protein 51)	NM_001706.2	–0.819	0.013	–0.74	1.67
PYGL[c]	phosphorylase, glycogen; liver (Hers disease, glycogen storage disease type VI)	NM_002863.2	–0.804	0.016	–0.74	1.67
cDNA clone fs01a03 5′	fs01a03y1 Human Lens cDNA (Normalized): fs cDNA clone fs01a03 5′	CD673362.1	–0.615	0.030	–0.73	1.66
602156641F1 NIH_MGC _83	602156641F1 NIH_MGC_83 cDNA clone IMAGE:4297258 5′	BF681513.1	–0.597	0.037	–0.73	1.66
CSNK2A1	casein kinase 2, α 1 polypeptide	NM_177560.2	–0.693	0.030	–0.73	1.66
KIAA0082	KIAA0082	NM_015050.1	–0.945	0.010	–0.72	1.65
UI-E-DW0-agh-c-03-0-UIr1 UI-E-DW0[c]	UI-E-DW0-agh-c-03-0-UIr1 UI-E-DW0 cDNA clone UI-E-DW0-agh-c-03-0-UI 5′	BM706230.1	–0.714	0.024	–0.72	1.65
CNTNAP1	contactin associated protein 1	NM_003632.1	–0.628	0.041	–0.72	1.64

Continued

TABLE 2—*Continued*

SYNGR1[b]	synaptogyrin 1	NM_004711.3	–0.635	0.043	–0.71	1.64
ING4	inhibitor of growth family, member 4	NM_198287.1	–0.586	0.044	–0.69	1.62
RBM5[b]	RNA binding motif protein 5	NM_005778.1	–0.71	0.024	–0.69	1.61
FLJ34274	cDNA FLJ34274 fis, clone FEBRA2003327	AK091593.1	–0.618	0.044	–0.68	1.60
FAM113A[b]	family with sequence similarity 113, member A	NM_022760.3	–0.796	0.015	–0.68	1.60
MAP3K6	mitogen-activated protein kinase kinase kinase 6	NM_004672.3	–0.584	0.041	–0.67	1.59
FLJ14360	hypothetical protein FLJ14360	NM_032775.2	–0.638	0.030	–0.67	1.59
B4GALT7[b]	xylosylprotein β 1,4-galactosyltransferase, polypeptide 7 (galactosyltransferase I)	NM_007255.1	–0.76	0.026	–0.66	1.57
CASP7[b]	caspase 7, apoptosis-related cysteine peptidase	NM_001227.2	–0.637	0.023	–0.65	1.57
IXL[b]	intersex-like (Drosophila)	AL137304.1	–0.662	0.031	–0.65	1.57
RHBDF2	rhomboid-like protein 6	NM_024599.2	–0.636	0.030	–0.65	1.57
UCN	urocortin	NM_003353.2	–0.625	0.044	–0.65	1.57
FLRT2	fibronectin leucine rich transmembrane protein 2	NM_013231.3	–0.595	0.042	–0.64	1.56
FLJ45129	cDNA FLJ45129 fis, clone BRAWH3037394	AK127072.1	–0.582	0.048	–0.63	1.55
LKAP[c]	limkain b1	NM_014647.1	–0.693	0.012	–0.63	1.55
yj34b04r1[b]	yj34b04r1 Soares placenta Nb2HP cDNA clone IMAGE:150607 5′	H02050.1	–0.722	0.017	–0.62	1.54
HECA[b]	headcase homolog (Drosophila)	NM_016217.1	–0.629	0.047	–0.62	1.54
BMP1[b]	bone morphogenetic protein 1	NM_006129.2	–0.763	0.024	–0.62	1.54
601194047F1 NIH_ MGC_7	601194047F1 NIH_MGC_7 cDNA clone IMAGE:3537995 5′	BE264943.1	–0.699	0.048	–0.62	1.54
TNIP2[b]	TNFAIP3 interacting protein 2	NM_024309.2	–0.95	0.008	–0.62	1.54
ZNF688	zinc finger protein 688	NM_145271.2	–0.669	0.026	–0.61	1.53
MITF	microphthalmia-associated transcription factor	NM_006722.1	–0.62	0.042	–0.60	1.51
FLJ45204[b]	cDNA FLJ45204 fis, clone BRCAN2009168	AK127147.1	–0.807	0.010	–0.60	1.51
UBXD7[c]	UBX domain containing 7	AB018337.1	–0.811	0.007	–0.58	1.50
C16orf48[b]	hypothetical protein DKFZp434A1319 (DKFZP434A1319)	NM_032140.1	–0.714	0.015	–0.58	1.50
ZFHX4	zinc finger homeodomain 4	NM_024721.2	–0.643	0.030	–0.58	1.49
yo60a08r1	yo60a08r1 Soares breast 3NbHBst cDNA clone IMAGE:182294 5′ similar to contains Alu repetitive element; contains LTR9 repetitive element	H41942.1	–0.692	0.031	–0.58	1.49
ZNF44	zinc finger protein 44	BC032246.1	–0.614	0.032	–0.57	1.49
SETD5	SET domain containing 5	AB051544.1	–0.6	0.031	–0.57	1.48
RNF103	ring finger protein 103	NM_005667.2	–0.648	0.031	–0.57	1.48
TP53INP1	tumor protein p53 inducible nuclear protein 1	NM_033285.2	–0.642	0.028	–0.55	1.47
yr35b01r1 Soares fetal liver spleen 1NFLS[b]	yr35b01r1 Soares fetal liver spleen 1NFLS cDNA clone IMAGE:207241 5′	H59642.1	–0.631	0.038	–0.55	1.46
BBS1	Bardet-Biedl syndrome 1	NM_024649.4	–0.616	0.047	–0.54	1.46
FLJ43900	cDNA FLJ43900 fis, clone TESTI4009973	AK125888.1	–0.669	0.043	–0.54	1.45
ITM2B[b]	integral membrane protein 2B	NM_021999.2	–0.681	0.028	–0.54	1.45
PDE6G[b]	phosphodiesterase 6G, cGMP-specific, rod, gamma	NM_002602.1	–0.87	0.003	–0.53	1.44

Continued

TABLE 2—*Continued*

FKBP4	FK506 binding protein 4, 59kDa	NM_002014.2	–0.697	0.023	–0.53	1.44
CHKB	choline kinase β (CHKB)	NM_005198.3	–0.593	0.039	–0.52	1.43
FLJ11946[b]	cDNA FLJ11946 fis, clone HEMBB1000709	AK022008.1	–0.922	0.005	–0.50	1.42
wi65f08×1 NCI_ CGAP_ Kid12	wi65f08×1 NCI_CGAP_Kid12 cDNA clone IMAGE:2398215 3′	AI763182.1	–0.621	0.044	–0.50	1.42
NSMAF[c]	neutral sphingomyelinase (N-SMase) activation associated factor	NM_003580.2	–0.789	0.015	–0.50	1.41
SIX5[b]	sine oculis homeobox homolog 5 (Drosophila)	NM_175875.3	–0.75	0.017	–0.49	1.40
64B2 Human retina cDNA Tsp509I-cleaved sublibrary[b]	64B2 Human retina cDNA Tsp509I-cleaved sublibrary Homo sapiens cDNA not directional	W22248.1	–0.684	0.022	–0.48	1.39
XPC	xeroderma pigmentosum, complementation group C	NM_004628.2	–0.644	0.041	–0.48	1.39
603040523F1 NIH_MGC_ 115	603040523F1 NIH_MGC_115 cDNA clone IMAGE:5181509 5′	BI824163.1	–0.708	0.030	–0.48	1.39
DKFZp686 K2137	mRNA; cDNA DKFZp686K2137 (from clone DKFZp686K2137)	AL833529.1	–0.626	0.037	–0.47	1.38
SRRM2	serine/arginine repetitive matrix 2	NM_016333.2	–0.632	0.042	–0.45	1.36
SH3GLB2	SH3-domain GRB2-like endophilin B2	NM_020145.2	–0.662	0.037	–0.45	1.36
yd89d12r1 Soares fetal liver spleen 1NFLS	yd89d12r1 Soares fetal liver spleen 1NFLS cDNA clone IMAGE:115415 5′	T87528.1	–0.592	0.050	–0.43	1.35
cDNA clone IMAGE: 3636922	cDNA clone IMAGE:3636922	BC062348.1	–0.598	0.035	–0.43	1.34
PTPRA	protein tyrosine phosphatase, receptor type, A	NM_002836.2	–0.624	0.042	–0.41	1.33
C20orf111	chromosome 20 open reading frame 111	NM_016470.6	–0.632	0.043	–0.41	1.33
MGAT1[b]	mannosyl (α-1,3-)-glycoprotein β-1,2-N-acetylglucosaminyltransferase	NM_002406.2	–0.799	0.019	–0.40	1.32
ZDHHC3[b]	zinc finger, DHHC domain containing 3	NM_016598.1	–0.634	0.040	–0.32	1.25
cDNA DKFZp 313K127[b]	mRNA; cDNA DKFZp313K127 (from clone DKFZp313K127)	AL833316.1	–0.74	0.024	–0.31	1.24
GANAB	glucosidase, alpha; neutral AB	NM_198334.1	–0.676	0.034	–0.31 x-fold up-regulated in Apert	1.24
NUBP2	nucleotide binding protein 2 (MinD homolog, E coli)	NM_012225.1	0.66	0.030	0.23	1.17
AGENCOURT_ 8454944 NIH_MGC_ 113	AGENCOURT_8454944 NIH_MGC_113 cDNA clone IMAGE:6278846 5′	BU899205.1	0.587	0.046	0.28	1.22
ATP5G1	ATP synthase, H + transporting, mitochondrial F0 complex, subunit C1 (subunit 9)	NM_005175.1	0.618	0.042	0.28	1.22

Continued

TABLE 2—*Continued*

AGENCOURT_8073800 NIH_MGC_110[b]	AGENCOURT_8073800 NIH_MGC_110 cDNA clone IMAGE:6083397 5′	BU147450.1	0.678	0.020	0.32	1.25
CIB1[b]	calcium and integrin binding 1 (calmyrin)	NM_006384.2	0.665	0.035	0.32	1.25
ARL3	ADP-ribosylation factor-like 3	NM_004311.2	0.633	0.033	0.34	1.27
PSMA2	proteasome (prosome, macropain) subunit, α type, 2	NM_002787.3	0.648	0.039	0.36	1.28
MAGED2[b]	melanoma antigen, family D, 2	NM_014599.4	0.599	0.030	0.36	1.28
CUTA	cutA divalent cation tolerance homolog (E. coli)	NM_015921.1	0.603	0.044	0.37	1.29
CSNK1D	casein kinase 1, delta	NM_001893.3	0.614	0.042	0.37	1.29
MTCH2	mitochondrial carrier homolog 2 (C elegans) (MTCH2), nuclear gene encoding mitochondrial protein	NM_014342.2	0.576	0.045	0.38	1.30
yp83b01s1 Soares fetal liver spleen 1NFLS	yp83b01s1 Soares fetal liver spleen 1NFLS cDNA clone IMAGE:193993 3′	H51256.1	0.597	0.049	0.38	1.30
MAPRE1	microtubule-associated protein, RP/EB family, member 1	NM_012325.1	0.613	0.045	0.38	1.30
SMARCA4	SWI/SNF related, matrix associated, actin dependent regulator of chromatin, subfamily a, member 4	NM_003072.2	0.658	0.034	0.39	1.31
PLA2G12A	phospholipase A2, group XIIA	NM_030821.3	0.668	0.044	0.39	1.31
METTL2B[b]	methyltransferase like 2	NM_018396.1	0.753	0.019	0.40	1.32
EEF1B2[c]	eukaryotic translation elongation factor 1 β 2	NM_001959.2	0.879	*0.011*	0.40	1.32
GABPB2	GA binding protein transcription factor, β subunit 2	NM_002041.2	0.664	0.027	0.40	1.32
ZNF414[b]	zinc finger protein 414	NM_032370.1	0.742	0.029	0.41	1.32
ADCY2[b]	adenylate cyclase 2 (brain)	NM_020546.1	0.665	0.028	0.41	1.33
CASP8AP2	CASP8 associated protein 2	NM_012115.2	0.621	0.049	0.41	1.33
TIMP3[c]	TIMP metallopeptidase inhibitor 3	BG104808.1	0.966	0.006	0.42	1.34
EIF4A1	eukaryotic translation initiation factor 4A	NM_001416.1	0.585	0.038	0.44	1.35
MUS81[b]	MUS81 endonuclease homolog (S. cerevisiae)	NM_025128.3	0.662	0.024	0.44	1.35
CCDC72	coiled-coil domain containing 72	NM_015933.1	0.694	0.030	0.44	1.36
SNRPD1	small nuclear ribonucleoprotein D1 polypeptide 16kDa	NM_006938.2	0.619	0.044	0.44	1.36
DTYMK	deoxythymidylate kinase	NM_012145.2	0.64	0.037	0.44	1.36
STX2[b]	syntaxin 2	NM_194356.1	0.745	0.019	0.44	1.36
AARSD1[b]	alanyl-tRNA synthetase domain containing 1	NM_025267.2	0.786	0.019	0.45	1.37
CREB3[b]	cAMP responsive element binding protein 3	NM_006368.4	0.743	0.023	0.46	1.38
COX4NB	neighbor of COX4 (NOC4)	NM_006067.3	0.593	0.030	0.47	1.38
PDZK6	PDZ domain containing 6	NM_015693.2	0.63	0.038	0.47	1.39
UBE2N	ubiquitin-conjugating enzyme E2N (UBC13 homolog, yeast)	NM_003348.3	0.584	0.037	0.48	1.39
PPIH	peptidyl prolyl isomerase H	NM_006347.3	0.676	0.025	0.48	1.40
SIKE	suppressor of IKK epsilon	NM_025073.1	0.584	0.048	0.50	1.41
TK1	thymidine kinase 1, soluble	NM_003258.1	0.685	0.028	0.50	1.41

Continued

TABLE 2—*Continued*

PAFAH1B3	platelet-activating factor acetylhydrolase, isoform Ib, γ subunit 29kDa	NM_002573.2	0.651	0.037	0.51	1.42
SFRS7[b]	splicing factor, arginine/serine-rich 7, 35kDa	NM_006276.36	0.705	0.028	0.52	1.44
PSMC5	proteasome (prosome, macropain) 26S subunit, ATPase, 5	NM_002805.4	0.624	0.043	0.53	1.44
yr11c06r1 Soares fetal liver spleen 1NFLS[b]	yr11c06r1 Soares fetal liver spleen 1NFLS cDNA clone IMAGE:204970 5′	H57392.1	0.742	0.015	0.53	1.44
C15orf29[b]	chromosome 15 open reading frame 29	NM_024713.1	0.793	0.011	0.53	1.44
GFOD2[c]	glucose-fructose oxidoreductase domain containing 2	NM_030819.2	0.745	0.019	0.53	1.45
HN1	hematological and neurological expressed 1	NM_001002032.1	0.683	0.045	0.54	1.46
DKFZp451H129	mRNA; cDNA DKFZp451H129 (from clone DKFZp451H129)	AL833295.1	0.649	0.035	0.54	1.46
CKLF[b]	chemokine-like factor	NM_016951.2	0.726	0.021	0.55	1.46
OBFC1	oligonucleotide/oligosaccharide-binding fold containing 1	NM_024928.3	0.688	0.027	0.55	1.46
VAMP4[b]	vesicle-associated membrane protein 4, transcript variant 1	NM_201994.1	0.744	0.010	0.55	1.46
RRM1	ribonucleotide reductase M1 polypeptide	NM_001033.2	0.612	0.045	0.55	1.46
PSME4[b]	proteasome (prosome, macropain) activator subunit 4	NM_014614.1	0.736	0.022	0.56	1.47
PLK3	polo-like kinase 3 (Drosophila)	NM_004073.2	0.642	0.036	0.57	1.48
MRPL35[b]	mitochondrial ribosomal protein L35	NM_016622.2	0.706	0.014	0.57	1.49
DLAT[b]	dihydrolipoamide S-acetyltransferase (E2 component of pyruvate dehydrogenase complex)	NM_001931.2	0.707	0.019	0.58	1.49
HIP2[b]	huntingtin interacting protein 2	NM_005339.3	0.723	0.017	0.58	1.49
C20orf7	chromosome 20 open reading frame 7	NM_199052.1	0.615	0.041	0.59	1.50
UFD1L[b]	ubiquitin fusion degradation 1 like (yeast)	NM_005659.3	0.616	0.023	0.59	1.51
POP5	processing of precursor 5, ribonuclease P/MRP subunit (S cerevisiae) (POP5)	NM_015918.3	0.623	0.041	0.59	1.51
SLC35B3	solute carrier family 35, member B3	NM_015948.2	0.628	0.037	0.60	1.51
CDKN3	cyclin-dependent kinase inhibitor 3 (CDK2-associated dual specificity phosphatase)	NM_005192.2	0.613	0.044	0.60	1.52
LZIC[b]	leucine zipper and CTNNBIP1 domain containing	NM_032368.3	0.766	0.019	0.60	1.52
LETM1	leucine zipper-EF-hand containing transmembrane protein 1	NM_012318.1	0.589	0.049	0.60	1.52
RNASEH2A[b]	ribonuclease H2, subunit A	NM_006397.2	0.869	0.011	0.60	1.52
NEDD1	neural precursor cell expressed, developmentally downregulated 1	NM_152905.2	0.643	0.041	0.62	1.53
CEP78	centrosomal protein 78kDa	AW962072.1	0.672	0.028	0.63	1.54
UI-H-BI0-aah-e-06-0-Uls1 NCI_ CGAP_ Sub1	UI-H-BI0-aah-e-06-0-Uls1 NCI_CGAP_ Sub1 cDNA clone IMAGE:2709227 3′	AW014009.1	0.597	0.037	0.63	1.55
CKAP2	cytoskeleton associated protein 2	NM_018204.2	0.644	0.037	0.66	1.58

Continued

TABLE 2—*Continued*

ACTR3B[b]	ARP3 actin-related protein 3 homolog B (yeast)	NM_020445.1	0.765	0.016	0.67	1.59
ELAVL1	ELAV (embryonic lethal, abnormal vision, Drosophila)-like 1 (Hu antigen R)	NM_001419.2	0.635	0.041	0.67	1.59
POLR3K[b]	polymerase (RNA) III (DNA directed) polypeptide K	NM_016310.2	0.802	0.013	0.69	1.61
PI4KII[b]	phosphatidylinositol 4-kinase type II	NM_018425.2	0.77	0.014	0.69	1.62
TMEM107[b]	transmembrane protein 107	NM_183065.1	0.739	0.022	0.70	1.62
BCAP29	B-cell receptor-associated protein 29	NM_018844.1	0.644	0.040	0.70	1.63
PRPS1L1[b]	phosphoribosyl pyrophosphate synthetase 1-like 1	NM_175886.2	0.728	0.022	0.71	1.63
MTFMT[b]	mitochondrial methionyl-tRNA formyltransferase	NM_139242.2	0.866	0.008	0.72	1.64
DDX49	DEAD (Asp-Glu-Ala-Asp) box polypeptide 49	NM_019070.3	0.61	0.046	0.73	1.66
RAD1[b]	RAD1 homolog (S. pombe)	NM_002853.2	0.71	0.018	0.73	1.66
CMTM5	CKLF-like MARVEL transmembrane domain containing 5	NM_138460.2	0.721	0.019	0.74	1.67
NEK6[b]	NIMA (never in mitosis gene a)-related kinase 6	NM_014397.3	0.715	0.017	0.74	1.67
K-EST0149992 L3SNU475[b]	K-EST0149992 L3SNU475 cDNA clone L3SNU475-29-H12 5′	CB108944.1	0.657	0.015	0.75	1.68
yx15f01s1 Soares melanocyte 2NbHM[b]	yx15f01s1 Soares melanocyte 2NbHM cDNA clone IMAGE:261817 3′	H99198.1	0.766	0.015	0.76	1.70
EXOSC9[b]	exosome component 9	NM_005033.1	0.721	0.021	0.76	1.70
UI-E-CI0-aah-e-03-0-UIr1 UI-E-CI0	UI-E-CI0-aah-e-03-0-UIr1 UI-E-CI0 cDNA clone UI-E-CI0-aah-e-03-0-UI 5′	BM690376.1	0.659	0.031	0.79	1.73
PTS	6-pyruvoyltetrahydropterin synthase	NM_000317.1	0.597	0.047	0.79	1.73
C14orf143	chromosome 14 open reading frame 143	NM_145231.1	0.629	0.047	0.79	1.73
UBE2T	HSPC150 protein similar to ubiquitin-conjugating enzyme	NM_014176.1	0.664	0.029	0.83	1.77
SAE1	SUMO-1 activating enzyme subunit 1	NM_005500.1	0.62	0.049	0.83	1.78
AURKB	aurora kinase B	NM_004217.1	0.692	0.031	0.84	1.79
ARSJ	arylsulfatase family, member J	AK027201.1	0.708	0.028	0.85	1.80
RRM2[b]	ribonucleotide reductase M2 polypeptide	NM_001034.1	0.781	0.019	0.86	1.81
BCL7A	B-cell CLL/lymphoma 7A	NM_020993.2	0.652	0.034	0.86	1.82
IVNS1ABP	influenza virus NS1A binding protein	NM_006469.2	0.66	0.035	0.87	1.82
NCAPG	non-SMC condensin I complex, subunit G	NM_022346.2	0.689	0.028	0.87	1.83
CENPM[c]	centromere protein M	NM_024053.2	0.693	0.006	0.87	1.83
C5orf13	chromosome 5 open reading frame 13	NM_004772.1	0.626	0.042	0.89	1.85
MCM4	MCM4 minichromosome maintenance deficient 4 (S. cerevisiae)	NM_182746.1	0.65	0.030	0.90	1.87
FLJ43294	cDNA FLJ43294 fis, clone MESTC1000042	AK125284.1	0.527	0.049	0.93	1.90
PTPDC1[b]	protein tyrosine phosphatase domain containing 1	NM_152422.3	0.725	0.027	0.95	1.93
LOC90624	hypothetical protein LOC90624	NM_181705.1	0.642	0.026	0.95	1.94
SPAG5[b]	sperm associated antigen 5	NM_006461.2	0.876	*0.007*	0.98	1.97
CTPS	CTP synthase	NM_001905.1	0.496	0.046	0.98	1.98
zu70f09r1 Soares_ testis_NHT	zu70f09r1 Soares_testis_NHT cDNA clone IMAGE:743369 5′	AA400694.1	0.578	0.039	0.99	1.98

Continued

TABLE 2—*Continued*

MND1	meiotic nuclear divisions 1 homolog (S. cerevisiae)	NM_032117.2	0.674	0.034	1.00	2.00
KIAA0101	KIAA0101 gene product	NM_014736.3	0.58	0.050	1.02	2.03
ZNF738[c]	zinc finger protein 738	BC034499.1	1.07	0.003	1.03	2.04
EHD4[c]	EH-domain containing 4	NM_139265.2	0.725	0.001	1.04	2.06
MNS1[b]	meiosis-specific nuclear structural 1	NM_018365.1	0.832	0.013	1.06	2.08
ARHGAP11A	similar to human GTPase-activating protein	NM_014783.2	0.7	0.027	1.08	2.12
CENPN[c]	centromere protein N	NM_018455.3	1.142	*0.001*	1.10	2.14
STMN1[b]	stathmin 1/oncoprotein 18	NM_203401.1	0.969	*0.006*	1.11	2.16
DUSP2[b]	dual specificity phosphatase 2	NM_004418.2	0.953	0.004	1.17	2.25
SPBC25[b]	spindle pole body component 25 homolog (S. cerevisiae)	NM_020675.3	0.892	0.010	1.18	2.27
HIST1H4C	histone 1, H4c	NM_003542.3	0.682	0.033	1.22	2.32
TCF19	transcription factor 19 (SC1)	BC033086.1	0.631	0.041	1.23	2.34
CIP29	cytokine induced protein 29 kDa	NM_033082.1	0.65	0.040	1.24	2.36
FLJ39342[b]	cDNA FLJ39342 fis, clone OCBBF2018873	AK096661.1	0.776	0.017	1.32	2.50
FLJ23131	cDNA: FLJ23131 fis, clone LNG08502	AK026784.1	0.645	0.039	1.61	3.05
zv03f03r1 Soares_ NhHMPu_ S1	zv03f03r1 Soares_NhHMPu_S1 cDNA clone IMAGE:752573 5′	AA419568.1	0.718	0.041	1.74	3.34
CNN1	calponin 1, basic, smooth muscle	NM_001299.3	0.808	0.022	2.09	4.24
HAPLN1[c]	hyaluronan and proteoglycan link protein 1	NM_001884.2	1.003	0.005	3.00	7.99

[a]SNR stands for "signal to noise ratio".
[b]The 120 genes identified as differentially expressed in at least 50% of the "leave-one-out" datasets.
[c]The 25 genes identified as differentially expressed in 100% of the "leave-one-out" datasets.

To improve the statistical significance and identify the most robust markers in the AS gene expression signature we performed a leave-one-out statistical analysis (detailed in Methods). Out of the 263 genes previously found to be differentially expressed, 120 genes were identified in at least 50 percent of the "leave-one-out" datasets, and 25 genes were present in all "leave-one-out" datasets (Tables 2 and 3).

Quantitative Real Time PCR Validation of Microarray Data

Quantitative real-time PCR (qRT-PCR) was performed to confirm the differential expression of gene sets identified in the microarray analysis. We selected for validation four genes belonging to the previously mentioned functional categories: *STMN1* and *SPAG5* (cell proliferation), *RRM2* (cell proliferation and nucleotide metabolism), and *HIP2* (suppression of apoptosis and regulation of gene expression). In addition, two other genes were selected with non-related functions: *CENPN* (centromere protein), and *EEF1B2* (translation elongation factor). The above selection was picked at random to avoid a bias toward a specific pathway in the validation of the microarray results. qRT-PCR experiments showed that these six genes were upregulated in AS cells (Figure 3), corroborating the expression results obtained in the microarray experiments.

FGF2 Treatment

To independently confirm the data generated by microarray analysis, and to mimic the increased downstream signaling caused by mutant FGFR2, primary cultured control periosteal cells were treated with a high concentration of FGF2 (the high concentration of FGF2 was used to simulate the phosphorylation status of mutant FGFR2c). Total RNA was isolated three, six, and 24 h after FGF2 addition. qRT-PCR was used to measure the changes in mRNA levels of the six genes previously used for experimental validation of the microarray data: *STMN1*, *SPAG5*, *RRM2*, *HIP2*, *CENPN and EEF1B2*. We observed that FGF2 treatment differentially stimulated the expression of these genes only after 24 h of treatment (Figure 4).

DISCUSSION

Despite the important role played by the periosteum in normal suture biology, the contribution of FGFR2 mutant periosteal cells in AS suture closure is unknown. We report here, for the first time, a strikingly higher osteoblast differentiation of heterozygous p.Ser252Trp FGFR2 mutant cells as compared with the same kind of cells from individuals without this mutation and normal suture fusion. To delineate molecular mechanisms underlying this abnormal cell behavior, we also present here a statistically significant difference in gene

Table 3. 98 genes grouped in functional categories. Transcripts are ordered by their Apert-to-control ratios (Log 2). Upregulated genes in AS cells are shown in orange. Downregulated genes are shown in blue.

Gene (Official Symbol)	Gene name	Accession number	*P* value	Apert-to-control Ratio (Log2)	x-fold up- or down-regulated in Apert
Positive regulation of cell proliferation					
CIP29	cytokine induced protein 29 kDa	NM_033082.1	0.040	1.24	2.36
TCF19	transcription factor 19 (SC1)	BC033086.1	0.041	1.23	2.34
SPBC25[b]	spindle pole body component 25 homolog (S. cerevisiae)	NM_020675.3	0.010	1.18	2.27
STMN1[b]	stathmin 1/oncoprotein 18	NM_203401.1	0.006	1.11	2.16
SPAG5[b]	sperm associated antigen 5	NM_006461.2	0.007	0.98	1.97
MCM4	MCM4 minichromosome maintenance deficient 4 (S. cerevisiae)	NM_182746.1	0.030	0.90	1.87
HCAP-G	chromosome condensation protein G	NM_022346.2	0.028	0.87	1.83
RRM2[b]	ribonucleotide reductase M2 polypeptide	NM_001034.1	0.019	0.86	1.81
AURKB	aurora kinase B	NM_004217.1	0.031	0.84	1.79
NEK6[b]	NIMA (never in mitosis gene a)-related kinase 6	NM_014397.3	0.017	0.74	1.67
CKAP2	cytoskeleton associated protein 2	NM_018204.2	0.037	0.66	1.58
NEDD1	neural precursor cell expressed, developmentally downregulated 1	NM_152905.2	0.041	0.62	1.53
RNASEH2A[b]	ribonuclease H2, subunit A	NM_006397.2	0.011	0.60	1.52
UFD1L[b]	ubiquitin fusion degradation 1 like (yeast)	NM_005659.3	0.023	0.59	1.51
PLK3	polo-like kinase 3 (Drosophila)	NM_004073.2	0.036	0.57	1.48
CKLF[b]	chemokine-like factor	NM_016951.2	0.021	0.55	1.46
TK1	thymidine kinase 1, soluble	NM_003258.1	0.028	0.50	1.41
DTYMK	deoxythymidylate kinase	NM_012145.2	0.037	0.44	1.36
MUS81[b]	MUS81 endonuclease homolog (S. cerevisiae)	NM_025128.3	0.024	0.44	1.35
MAPRE1	microtubule-associated protein, RP/EB family, member 1	NM_012325.1	0.045	0.38	1.30
HECA[b]	headcase homolog (Drosophila)	NM_016217.1	0.047	–0.62	1.54
CSNK2A1	casein kinase 2, α 1 polypeptide	NM_177560.2	0.030	–0.73	1.66
BCL6[a]	B-cell CLL/lymphoma 6 (zinc finger protein 51)	NM_001706.2	0.013	–0.74	1.67
BCL3	B-cell CLL/lymphoma 3	NM_005178.2	0.039	–0.79	1.73
ADAM33	ADAM metallopeptidase domain 33	NM_153202.1	0.027	–1.22	2.33
PDGFRA	platelet-derived growth factor receptor, α polypeptide	NM_006206.2	0.045	–1.34	2.53
ChGn[a]	chondroitin beta1,4 N-acetylgalactosaminyltransferase	NM_018371.3	0.015	–1.42	2.68
PIK3C2B[a]	phosphoinositide-3-kinase, class 2, β polypeptide	NM_002646.2	0.004	–1.54	2.91
Negative regulation of cell proliferation					
RAD1[b]	RAD1 homolog (S. pombe)	NM_002853.2	0.018	0.73	1.66
CDKN3	cyclin-dependent kinase inhibitor 3 (CDK2-associated dual specificity phosphatase)	NM_005192.2	0.044	0.60	1.52
RBM5[b]	RNA binding motif protein 5	NM_005778.1	0.024	–0.69	1.61
ING4	inhibitor of growth family, member 4	NM_198287.1	0.044	–0.69	1.62
IFITM3	interferon induced transmembrane protein 3 (1-8U)	NM_021034.1	0.033	–0.83	1.77
KLF11	Kruppel-like factor 11	NM_003597.4	0.039	–0.92	1.89
MTSS1[b]	metastasis suppressor 1	NM_014751.2	0.009	–1.14	2.20
RARRES3[b]	retinoic acid receptor responder (tazarotene induced) 3	NM_004585.2	0.022	–1.64	3.12
Nucleotide metabolism					
CTPS	CTP synthase	NM_001905.1	0.046	0.98	1.98
RRM2[b]	ribonucleotide reductase M2 polypeptide	NM_001034.1	0.019	0.86	1.81
PRPS1L1[b]	phosphoribosyl pyrophosphate synthetase 1-like 1	NM_175886.2	0.022	0.71	1.63
POLR3K[b]	polymerase (RNA) III (DNA directed) polypeptide K	NM_016310.2	0.013	0.69	1.61
RRM1	ribonucleotide reductase M1 polypeptide	NM_001033.2	0.045	0.55	1.46
TK1	thymidine kinase 1, soluble	NM_003258.1	0.028	0.50	1.41
DTYMK	deoxythymidylate kinase	NM_012145.2	0.037	0.44	1.36

Continued

TABLE 3—*Continued*

ADCY2[b]	adenylate cyclase 2 (brain)	NM_020546.1	0.028	0.41	1.33
ATP5G1	ATP synthase, H + transporting, mitochondrial F0 complex, subunit C1 (subunit 9)	NM_005175.1	0.042	0.28	1.22
PDE6G[b]	phosphodiesterase 6G, cGMP-specific, rod, gamma	NM_002602.1	0.003	–0.53	1.44
Regulation of gene expression					
CIP29	cytokine induced protein 29 kDa	NM_033082.1	0.040	1.24	2.36
ZNF738[a]	zinc finger protein 738	BC034499.1	0.003	1.03	2.04
POLR3K[b]	polymerase (RNA) III (DNA directed) polypeptide K	NM_016310.2	0.013	0.69	1.61
ELAVL1	ELAV (embryonic lethal, abnormal vision, Drosophila)-like 1 (Hu antigen R)	NM_001419.2	0.041	0.67	1.59
HIP2[b]	huntingtin interacting protein 2	NM_005339.3	0.017	0.58	1.49
CREB3[b]	cAMP responsive element binding protein 3	NM_006368.4	0.023	0.46	1.38
CASP8AP2	CASP8 associated protein 2	NM_012115.2	0.049	0.41	1.33
ZNF414[b]	zinc finger protein 414	NM_032370.1	0.029	0.41	1.32
GABPB2	GA binding protein transcription factor, β subunit 2	NM_002041.2	0.027	0.40	1.32
SMARCA4	SWI/SNF related, matrix associated, actin dependent regulator of chromatin, subfamily a, member 4	NM_003072.2	0.034	0.39	1.31
SIX5[b]	sine oculis homeobox homolog 5 (Drosophila)	NM_175875.3	0.017	–0.49	1.40
ZNF44	zinc finger protein 44	BC032246.1	0.032	–0.57	1.49
ZFHX4	zinc finger homeodomain 4	NM_024721.2	0.030	–0.58	1.49
MITF	microphthalmia-associated transcription factor	NM_006722.1	0.042	–0.60	1.51
ZNF688	zinc finger protein 688	NM_145271.2	0.026	–0.61	1.53
TNIP2[b]	TNFAIP3 interacting protein 2	NM_024309.2	0.008	–0.62	1.54
ING4	inhibitor of growth family, member 4	NM_198287.1	0.044	–0.69	1.62
BCL6[a]	B-cell CLL/lymphoma 6 (zinc finger protein 51)	NM_001706.2	0.013	–0.74	1.67
ELL3[b]	elongation factor RNA polymerase II-like 3	NM_025165.1	0.006	–0.74	1.67
PPARA[b]	peroxisome proliferative activated receptor, α	NM_032644.1	0.009	–0.74	1.67
RELB	v-rel reticuloendotheliosis viral oncogene homolog B, nuclear factor of kappa light polypeptide gene enhancer in B-cells 3 (avian)	NM_006509.2	0.033	–0.74	1.67
ZFP64[b]	zinc finger protein 64 homolog (mouse)	NM_018197.2	0.017	–0.78	1.72
BCL3	B-cell CLL/lymphoma 3	NM_005178.2	0.039	–0.79	1.73
NFIL3[b]	nuclear factor, interleukin 3 regulated	NM_005384.1	0.012	–0.83	1.77
ANKZF1	ankyrin repeat and zinc finger domain containing 1	NM_018089.1	0.036	–0.85	1.81
ARID5A	AT rich interactive domain 5A (MRF1-like)	NM_006673.2	0.042	–0.92	1.89
KLF11	Kruppel-like factor 11	NM_003597.4	0.039	–0.92	1.89
CREB5[b]	cAMP responsive element binding protein 5	NM_004904.1	0.010	–1.00	2.00
PNRC1[a]	proline-rich nuclear receptor coactivator 1	NM_006813.1	0.008	–1.05	2.07
ATF3	activating transcription factor 3	NM_004024.2	0.049	–1.10	2.14
MAF	v-maf musculoaponeurotic fibrosarcoma oncogene homolog (avian)	NM_005360.2	0.044	–1.19	2.29
ZNF385[b]	zinc finger protein 385	NM_015481.1	0.011	–1.38	2.61
Cell Adhesion					
HAPLN1[a]	hyaluronan and proteoglycan link protein 1	NM_001884.2	0.005	3.00	7.99
CIB1[b]	calcium and integrin binding 1 (calmyrin)	NM_006384.2	0.035	0.32	1.25
FLRT2	fibronectin leucine rich transmembrane protein 2	NM_013231.3	0.042	–0.64	1.56
CNTNAP1	contactin associated protein 1	NM_003632.1	0.041	–0.72	1.64
CSNK2A1	casein kinase 2, α 1 polypeptide	NM_177560.2	0.030	–0.73	1.66
LGALS3BP[b]	lectin, galactoside-binding, soluble, 3 binding protein	NM_005567.2	0.014	–0.89	1.85
PERP	PERP, TP53 apoptosis effector	NM_022121.2	0.042	–0.92	1.89
ADAM8[b]	a disintegrin and metalloproteinase domain 8	NM_001109.1	0.044	–1.06	2.08
CLDN15[b]	claudin 15	NM_014343.1	0.022	–1.13	2.19
ADAM33	ADAM metallopeptidase domain 33	NM_153202.1	0.027	–1.22	2.33
PDGFRA	platelet-derived growth factor receptor, α polypeptide	NM_006206.2	0.045	–1.34	2.53

Continued

TABLE 3—*Continued*

TNXB[b]	tenascin XB	NM_032470.2	0.015	–2.32	4.98
DKFZp434 B1231[b]	eEF1A2 binding protein	NM_178275.3	0.010	–2.66	6.31
Extracellular matrix component, biosynthesis					
HAPLN1[a]	hyaluronan and proteoglycan link protein 1	NM_001884.2	0.005	3.00	7.99
TIMP3[a]	TIMP metallopeptidase inhibitor 3	BG104808.1	0.006	0.42	1.34
BMP1[b]	bone morphogenetic protein 1	NM_006129.2	0.024	–0.62	1.54
B4GALT7[b]	xylosylprotein β 1,4-galactosyltransferase, polypeptide 7 (galactosyltransferase I)	NM_007255.1	0.026	–0.66	1.57
MATN2	matrilin 2	NM_030583.1	0.027	–0.96	1.95
ChGn[a]	chondroitin beta1,4 N-acetylgalactosaminyltransferase	NM_018371.3	0.015	–1.42	2.68
TNXB[b]	tenascin XB	NM_032470.2	0.015	–2.32	4.98
MAPK signaling pathway					
DUSP2[b]	dual specificity phosphatase 2	NM_004418.2	0.004	1.17	2.25
STMN1[b]	stathmin 1/oncoprotein 18	NM_203401.1	0.006	1.11	2.16
PLA2G12A	phospholipase A2, group XIIA	NM_030821.3	0.044	0.39	1.31
PDE6G[b]	phosphodiesterase 6G, cGMP-specific, rod, gamma	NM_002602.1	0.003	–0.53	1.44
TNIP2[b]	TNFAIP3 interacting protein 2	NM_024309.2	0.008	–0.62	1.54
UCN	urocortin	NM_003353.2	0.044	–0.65	1.57
CASP7[b]	caspase 7, apoptosis-related cysteine peptidase	NM_001227.2	0.023	–0.65	1.57
MAP3K6	mitogen-activated protein kinase kinase kinase 6	NM_004672.3	0.041	–0.67	1.59
BCL3	B-cell CLL/lymphoma 3	NM_005178.2	0.039	–0.79	1.73
MAPK8IP1	mitogen-activated protein kinase 8 interacting protein 1	NM_005456.2	0.037	–0.86	1.81
SPTBN1	spectrin, beta, non-erythrocytic 1 (SPTBN1)	NM_003128.1	0.049	–0.87	1.83
KLF11	Kruppel-like factor 11	NM_003597.4	0.039	–0.92	1.89
PNRC1[a]	proline-rich nuclear receptor coactivator 1	NM_006813.1	0.008	–1.05	2.07
PDGFRA	platelet-derived growth factor receptor, α polypeptide	NM_006206.2	0.045	–1.34	2.53
PIK3C2B[a]	phosphoinositide-3-kinase, class 2, β polypeptide	NM_002646.2	0.004	–1.54	2.91
RARRES3[b]	retinoic acid receptor responder (tazarotene induced) 3	NM_004585.2	0.022	–1.64	3.12

[a]Genes within the list of 120 genes identified as differentially expressed in at least 50 percent of the "leave-one-out" datasets.
[b]Those within the list of 25 genes identified as differentially expressed in 100 percent of the "leave-one-out" datasets (see Methods for details).

expression profile of periosteal cells from a large group of AS patients (p.Ser252Trp mutation) as compared with normal FGFR2 expressing cells.

Our study represents the largest sample where a dominant gain-of-function mutation of a rare Mendelian disorder is analyzed through microarray technology. Successful detection of a gene expression signature was achieved possibly because all the patients harbor a common mutation in a tyrosine kinase receptor involved in critical developmental signaling cell pathways that leads to a very homogeneous phenotype. On the other hand, our sample size contrasts with the expression profile studies of complex disorders, such as cancer, which are etiologically very heterogeneous and require an even larger number of individuals in the analysis. It will be important to verify whether other craniosynostotic conditions with either known or unknown causative mutations are also correlated with specific gene expression signatures.

Lemonnier et al. (12) reported that AS p.Ser252Trp mutation induces striking downregulation of FGFR2 protein in osteoblasts, which was attributed to an increased internalization of the receptor. In contrast, our results indicate that AS periosteal cells have a different pattern of FGFR2 expression, as similar FGFR2 transcript and protein levels were observed between control and AS periosteal cells. These discrepancies may be due to differences between the two cell types used in the studies.

Independent confirmation of AS expression changes identified by our microarray studies came from three strategies. First we used qRT-PCR to confirm the upregulation of six genes (*STMN1*, *SPAG5*, *RRM2*, *HIP2*, *CENPN*, *EEF1B2*) in AS cell lines. As a second approach, we used control periosteal cells treated with high concentrations of exogenous FGF2 (a specific wild type FGFR2c ligand) to mimic the activation status of mutant FGFR2. We observed over-expression in FGF2-treated cells of the six genes previously confirmed to be upregulated in AS cells through qRT-PCR. Curiously, we observed a change in gene expression of the selected genes only after 24 h of FGF2 treatment, suggesting that their expression is a late event of FGFR2c activation. In addition, these results imply that the genes differentially expressed in the AS cells are involved either directly or

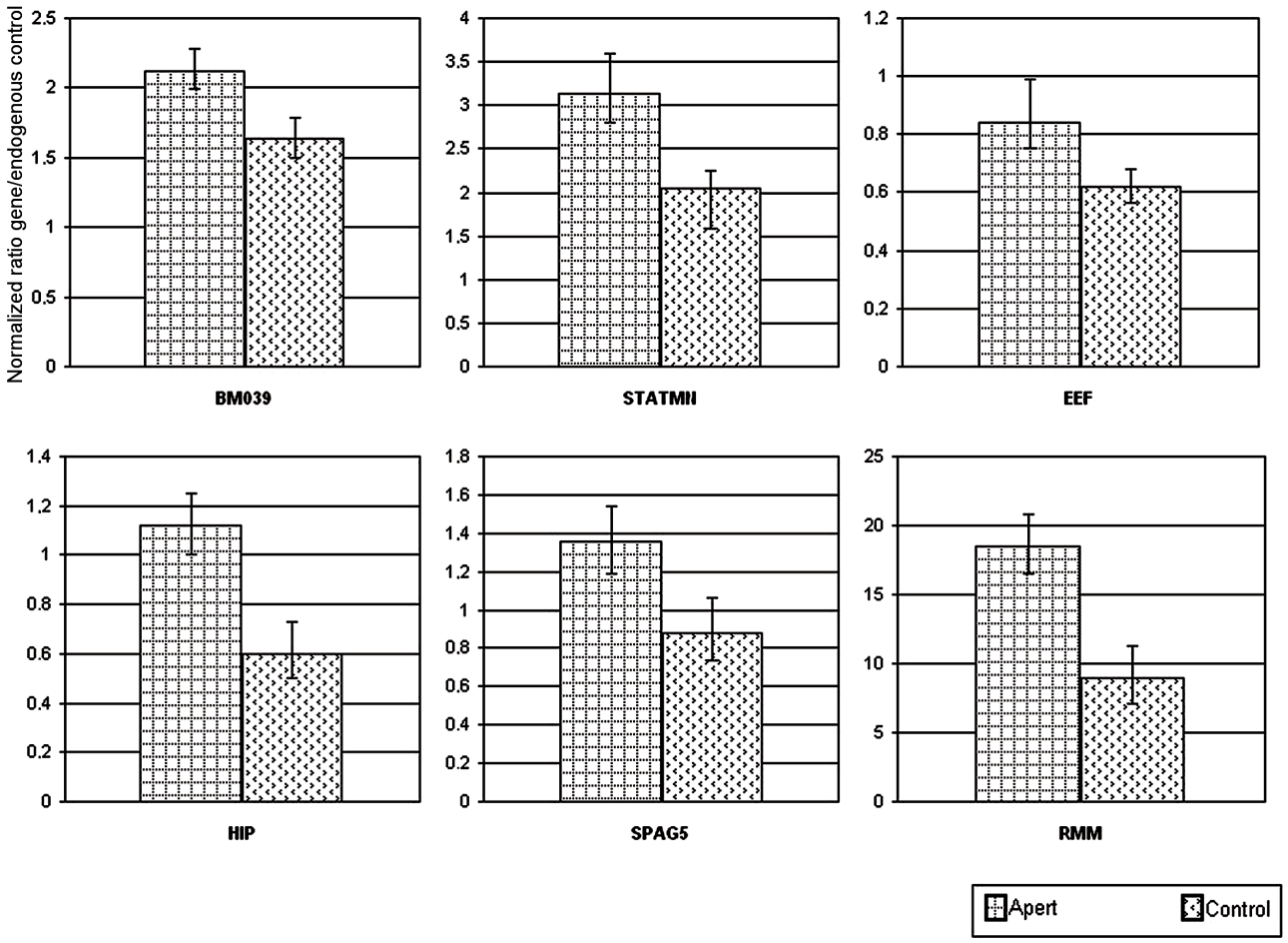

Figure 3. Real-time PCR showing expression levels for six genes identified as upregulated in AS cells by microarray analysis: *STMN1*, *SPAG5*, *RRM2*, *HIP2*, *CENPN*, *and EEF1B2*. The expression levels for these genes are enhanced in AS samples when compared with controls.

indirectly with FGFR2c signaling. It is important to point out that this strategy replicates the microarray data in a biologically analogous system. Indeed, Mansukhani et al. (15) showed that gene expression profiles of a murine osteoblast cell line harboring the p.Ser252Trp mutation could be reproduced by exogenous FGF treatment. These findings also suggest that the mutated FGFR2 may over-activate the normal molecular pathways elicited by wild type receptor instead of inducing novel molecular pathways.

As a third approach to validate our microarray results, we looked at the differentially expressed transcripts for genes known to be involved in the canonical FGFR transduction signaling pathways. As will be discussed later, we observed the presence of *PIK3C2B* gene, which encodes a protein of the phosphoinositide 3-kinase (PI3K) family, and of several members of the MAPK cascades. One of the important signaling pathways leading to activation of the MAP kinases is through FGFR-PI3K hierarchical cascade. We also observed different expression profiles concerning other genes associated with FGFR2 activation, such as *FLRT2*, a positive regulator of FGFR cascade, and *MITF*, a transcription factor acting downstream of FGFR/MEK/ERK signaling. Therefore, our results (including both laboratory and the leave-one-out statistical analysis) support that the expression signature observed in AS cells do represent a biological state caused by p.Ser252Trp mutation in FGFR2.

Analysis of the genes differentially expressed in AS cells revealed novel expression networks and cellular processes possibly involved in AS pathogenesis. A previous study reported a gene expression profiling experiment using fibroblast periosteal cells obtained from one AS patient (p.Pro253Arg), and two controls (20). We did not observe overlap between the list of genes identified in that study and the set of 263 genes reported here. We think that the very small number of samples analyzed in the previous study (one AS patient and two controls) may have introduced a considerable bias due to individual variation in gene expression, which

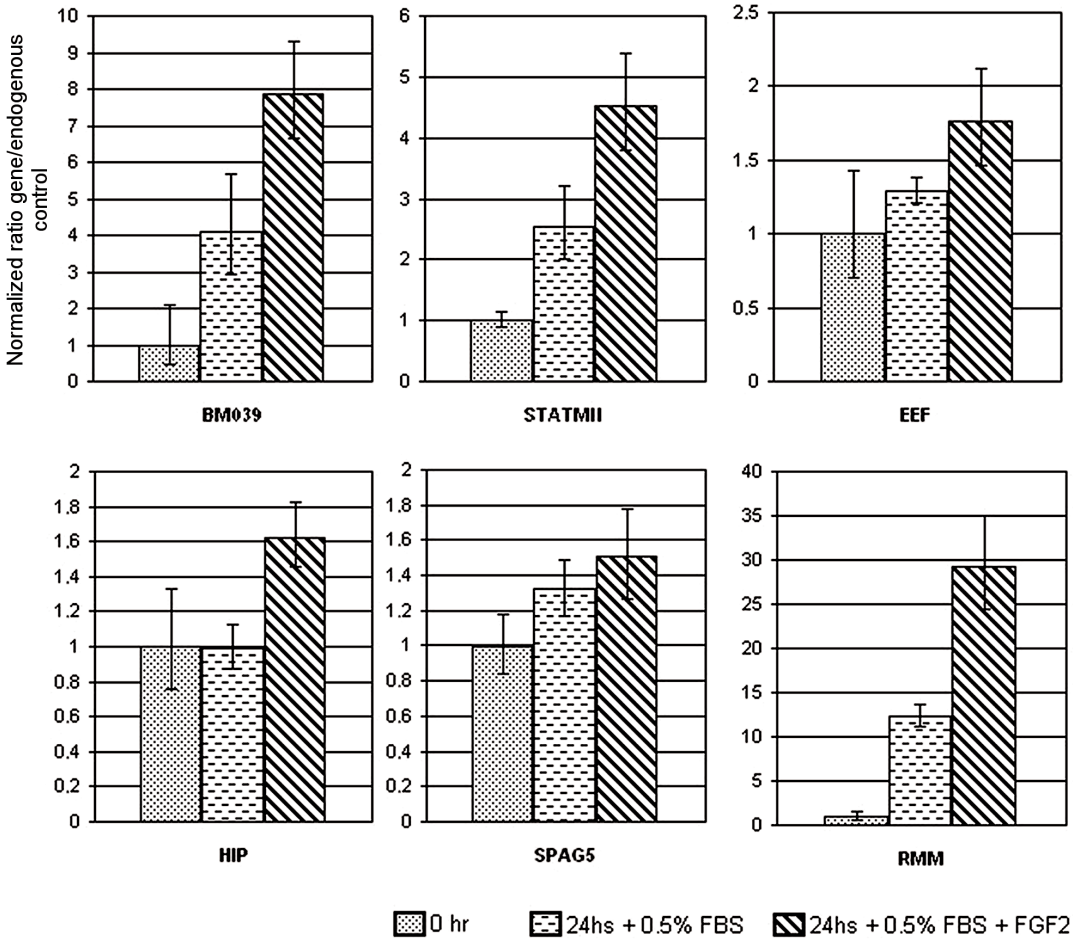

Figure 4. Real-time PCR showing expression levels for six genes (*STMN1, SPAG5, RRM2, HIP2, CENPN, and EEF1B2*) in response to FGF2 treatment. The bars are representing the expression levels of each gene before administration of 0.5 percent FBS and FGF2 (0 h), after 24 h of administration of 0.5 percent FBS (0.5 percent FBS) and after addition of 0.5 percent FBS and FGF2 (0.5 percent FBS + FGF2).

would explain the absence of genes in common in the two studies.

The majority of genes upregulated in AS cells are associated with positive regulation of cell proliferation and nucleotide metabolism, suggesting that the activating FGFR2 mutation induces increased periosteal cell proliferation. Indeed, an excessive proliferation in AS cells in comparison to control cells was clearly evident during tissue culture cell expansion although further experiments are needed to confirm this phenotype.

FGFR-MAPK signaling functions as a trigger of fibroblast cell proliferation. However, we observed downregulation of several members of MAPK signaling cascades (13 out of 16 genes) as well as *PIK3C2B* in AS cells. It is of note that among the three upregulated genes belonging to the MAPK cascades is *DUSP2*, which is associated with inhibition of MAPK signaling by dephosphorylating activated MAPKs. Interestingly, downregulation of PI3K and MAPK signaling pathways have been associated recently with increased stem cell differentiation (26,27). Therefore, it is possible that the AS mutant FGFR2 expressing cells are more committed toward the osteoblast lineage due to downregulation of transcripts associated with PIK3-MAPK signaling networks. However, further experiments to measure transcript/protein levels of components of the PIK3-MAPK pathway in mutant FGFR2 expressing cells are warranted to confirm the downregulation and the association of this signaling network with the pathophysiology of AS.

We also found downregulation of most of the genes involved in cell adhesion (11 out of 13 genes) and extracellular matrix composition (five out of seven genes) in AS cells, which contrast one previous study that has shown that periosteal AS cells synthesize a greater amount of extracellular matrix components (including glycosaminoglycans, type I and III collagens, and fibronectin) than normal cells (28). In view of this, it would be interesting to test if the suggested reduction in

cell adhesion and extracellular matrix complexity of our AS periosteal cells are associated with the greater osteogenic capacity of these cells.

As we are aware, the number of significantly altered genes (263 with a $P \leq 0.05$) does not exceed the expected number of genes that would be found by chance in the dataset using the same confidence interval (476 genes out of 9,526 by chance alone at $P \leq 0.05$, and a one-tailed distribution). However, if we took into account the 120 more significant genes (identified as differentially expressed in at least 50 percent of the "leave-one-out" datasets), we did not observe great differences in the distribution of the upregulated and downregulated genes among the functional categories previously discussed for the 263 genes. The exception is the group of genes associated with apoptosis, in which a tendency of enhancement of the number of genes downregulated in AS cells as compared with control cells was observed. These results thus confirm that the most abundant classes of upregulated genes are those related to positive regulation of cell proliferation and nucleotide metabolism, whereas the genes associated with all the other functional categories are mostly downregulated in AS cells.

It was reported that under osteogenic differentiation condition, murine calvarial osteoblast cells heterozygous for p.Ser252Trp mutation in FGFR2 showed increased apoptosis (13,15,16). However, we found an inclination toward downregulation of genes associated with apoptosis between control and AS cells among the 120 genes referred above; in fact, we did not observe significant cell death either in control or in the mutant cell lineages. These discrepancies may be due to differences in the experimental models and cell types used in each study.

Taken together, our findings have important implications in understanding the periosteum function in the postnatal pathogenesis of Apert syndrome patients. The increased proliferative and osteogenic potentials here observed in the AS cells may lead to an expansion of periosteal cells with the potential to differentiate and contribute to premature suture ossification. It is important to note that a similar mechanism already has been discussed for osteoblast cells upon FGFR over-activation (15). Injuries at the suture site, as those induced by surgical repair, could trigger this abnormal periosteal cell behavior and lead to acceleration of the suture fusion after surgery. Thus, our results suggest for the first time that the mutant periosteal cells in AS patients might play an important role in the pathogenesis of this disease as well as in the recurrent suture closure after surgery.

Recently, identification of mutations in *ephrin-B1* gene associated with craniosynostosis have led to the hypothesis that alteration in the cellular pathways activated by these molecules can lead to an abnormal compartmentalization of the cells during embryogenesis leading to disturbed tissue boundary formation (29). Considering the enhanced osteogenic potential of the AS periosteal cells and also that ephrins recently were shown to activate FGFRs (30), we would like to suggest that a similar mechanism may contribute to the craniosynostosis in FGFR-mutated patients, once the signals that determine separate identities of the cranial suture tissues have been disturbed.

While the full spectrum of molecular factors that modulate these aberrant cellular behaviors remains to be determined, our gene expression profiling study shall contribute to the identification of novel genes with important roles in ossification of cranial sutures or as candidates for syndromic craniosynostosis with still unidentified cause. Of particular note is the recent finding showing that loss of *Dusp6*, a member of the DUSP (dual-specificity phosphatases) family which is activated by FGFRs and inhibits MAP Kinases, cause coronal craniosynostosis in mice (31). Therefore DUSP family members may be considered good candidate genes for FGFR-like craniosynostosis. Interestingly, we found that *DUSP2* is one of the most significant differentially expressed genes in AS periosteal cells. Finally, the understanding of the molecular pathways involved in the abnormal AS periosteum behavior will certainly have important implications in the prognostic of surgical repair in syndromic craniosynostosis.

ACKNOWLEDGMENTS

We are grateful to all of the patients and their relatives who participated in this work. We would like to thank Dr Hugo Armelin and Jaqueline Salotti for providing the FGFR2 antibodies and Y1 cell lineage; Regina Maki Sasahara for her help in earlier phases of the project; Dr Oswaldo Keith Okamoto for stimulating and useful discussions; Constância G Urbani for secretarial assistance; Eder Zuconni and Natassia Vieira for their contribution to the flow citometry experiments; Dr Alessandra S Gordonos and Fernanda Jehee for revision of the manuscript. This work is supported by grants from Fundação de Amparo à Pesquisa do Estado de São Paulo (FAPESP) and Conselho Nacional de Desenvolvimento Científico e Tecnológico (CNPq).

REFERENCES

1. Cohen MM Jr et al. (1992) Birth prevalence study of the Apert syndrome. *Am. J. Med. Genet*. 42: 655–9.
2. Upton J, Zuker RM (eds) (1991) *Clinics in plastic surgery*. Vol 18: Apert syndrome. WB Saunders, Philadelphia.
3. Park WJ et al. (1995) Analysis of phenotypic features and FGFR2 mutations in Apert syndrome. *Am. J. Hum. Genet*. 57:321–8.
4. Slaney SF, et al. (1996) Differential effects of FGFR2 mutations on syndactyly and cleft palate in Apert syndrome. *Am. J. Hum. Genet*. 58:923–32.
5. Cohen MM Jr. (2000) Syndromes with craniosynostosis. In: Cohen Jr MM, MacLean RE. (eds) *Craniosynostosis: Diagnosis, Evaluation, and Management*. New York: Oxford University Press. 309–441.
6. Moloney DM et al. (1996) Exclusive paternal origin of new mutations in Apert syndrome. *Nat. Genet*., 13:48–53.
7. Wilkie AO et al. (1995) Apert syndrome results from localized mutations of FGFR2 and is allelic with Crouzon syndrome. *Nat. Genet*. 9:165–72.
8. Anderson J, Burns HD, Enriquez-Harris P, Wilkie AO, Heath JK. (1998) Apert syndrome mutations in fibroblast growth factor receptor 2 exhibit increased affinity for FGF ligand. *Hum. Mol. Genet*. 7:1475–83.
9. Yu K, Herr AB, Waksman G, Ornitz DM. (2000) Loss of fibroblast growth factor receptor 2 ligand-

binding specificity in Apert syndrome. *Proc. Natl. Acad. Sci. U. S. A.* 7:14536–41.
10. Ibrahimi OA, Zhang F, Hrstka SC, Mohammadi M, Linhardt RJ. (2004) Kinetic model for FGF, FGFR, and proteoglycan signal transduction complex assembly. *Biochemistry*. 43:4724–30.
11. Lomri A, Lemonnier J, Hott M, et al. (1998) Increased calvaria cell differentiation and bone matrix formation induced by fibroblast growth factor receptor 2 mutations in Apert syndrome. *J. Clin. Invest*. 101:1310–7.
12. Lemonnier J, Delannoy Ph, Hott M, Lomri A, Modrowski D, Marie PJ. (2000) The Ser252Trp fibroblast growth factor receptor-2 (FGFR-2) mutation induces PKC-independent downregulation of FGFR-2 associated with premature calvaria osteoblast differentiation. *Exp. Cell Res*. 256:158–67.
13. Mansukhani A, Bellosta P, Sahni M, Basilico C. (2000) Signaling by fibroblast growth factors (FGF) and fibroblast growth factor receptor 2 (FGFR2)-activating mutations blocks mineralization and induces apoptosis in osteoblasts. *J. Cell Biol*. 149: 1297–1308.
14. Lomri A, Lemonnier J, Delannoy P, Marie PJ. (2001) Increased expression of protein kinase Calpha, interleukin-1alpha, and RhoA guanosine 5′-triphosphatase in osteoblasts expressing the Ser252Trp fibroblast growth factor 2 receptor Apert mutation: identification by analysis of complementary DNA microarray. *J. Bone Miner. Res*. 16:705–12.
15. Mansukhani A, Ambrosetti D, Holmes G, Cornivelli L, Basilico C. (2005) Sox2 induction by FGF and FGFR2 activating mutations inhibits Wnt signaling and osteoblast differentiation. *J. Cell Biol*. 168:1065–76.
16. Chen L, Li D, Li C, Engel A, Deng CX. (2005) A Ser252Trp [corrected] substitution in mouse fibroblast growth factor receptor 2 (Fgfr2) results in craniosynostosis. *Bone*. 33:169–78. Erratum in: *Bone*. (2005) 37:876.
17. Wang Y et al. (2005) Abnormalities in cartilage and bone development in the Apert syndrome FGFR2(+/S252W) mouse. *Development*. 132: 3537–48.
18. Hopper RA et al. (2001) Effect of isolation of periosteum and dura on the healing of rabbit calvarial inlay bone grafts. *Plast. Reconstr. Surg*. 107:454–62
19. Ozerdem OR et al. (2003) Roles of periosteum, dura, and adjacent bone on healing of cranial osteonecrosis. *J. Craniofac. Surg*.14:371–9.
20. Carinci F et al. (2002) Expression profiles of craniosynostosis-derived fibroblasts. *Mol. Med*. 8: 638–44.
21. Zuk PA et al. (2001) Multilineage cells from human adipose tissue: implications for cell-based therapies. *Tissue Eng*. 7:211–28.
22. Quackenbush J. (2002) Microarray data normalization and transformation. *Nat Genet*. 32(Suppl.):496–501.
23. Golub TR et al. (1999) Molecular classification of cancer: class discovery and class prediction by gene expression monitoring. *Science*. 286:531–7.
24. Reis EM et al. (2004) Antisense intronic non-coding RNA levels correlate to the degree of tumor differentiation in prostate cancer. *Oncogene*. 23:6684–92.
25. van't Veer LJ et al. (2002) Gene expression profiling predicts clinical outcome of breast cancer. *Nature*. 415:530–6.
26. Takahashi K, Murakami M, Yamanaka S. (2005) Role of the phosphoinositide 3-kinase pathway in mouse embryonic stem (ES) cells. *Biochem. Soc. Trans*. 33:522–5.
27. Armstrong L et al. (2006) The role of PI3K/AKT, MAPK/ERK and NFkappabeta signaling in the maintenance of human embryonic stem cell pluripotency and viability highlighted by transcriptional profiling and functional analysis. *Hum. Mol. Genet*. 15:1894–1913.
28. Bodo M et al. (1997) Glycosaminoglycan metabolism and cytokine release in normal and otosclerotic human bone cells interleukin-1 treated. *Eur. J. Clin. Invest*. 27:36–42.
29. Twigg SR et al. (2004) Mutations of ephrin-B1 (EFNB1), a marker of tissue boundary formation, cause craniofrontonasal syndrome. *Proc. Natl. Acad. Sci. U S A*. 101:8652–7.
30. Yokote H et al. (2005) Trans-activation of EphA4 and FGF receptors mediated by direct interactions between their cytoplasmic domains. *Proc. Natl. Acad. Sci. U. S. A*. 102:8866–71.
31. Li C, Scott DA, Hatch E, Tian X, Mansour SL. (2007) Dusp6 (Mkp3) is a negative feedback regulator of FGF-stimulated ERK signaling during mouse development. *Development*. 134:167–76.